Geophysical Research Letters

RESEARCH LETTER
10.1029/2023GL107634

An Inconsistent ENSO Response to Northern Hemisphere Stadials Over the Last Deglaciation

Ryan H. Glaubke[1,2], Matthew W. Schmidt[1], Jennifer E. Hertzberg[1], Lenzie G. Ward[1], Franco Marcantonio[3], Danielle Schimmenti[3], and Kaustubh Thirumalai[4]

[1]Department of Ocean and Earth Sciences, Old Dominion University, Norfolk, VA, USA, [2]Department of Marine and Coastal Sciences, Rutgers University, New Brunswick, NJ, USA, [3]Department of Geology and Geophysics, Texas A&M University, College Station, TX, USA, [4]Department of Geosciences, University of Arizona, Tucson, AZ, USA

Key Points:

- Single-shell foraminiferal trace element ratios reveal a deglacial history of El Niño-Southern Oscillation's (ENSO) variability from the eastern equatorial Pacific
- Meltwater-induced changes to ocean and atmospheric circulation likely amplified ENSO during Heinrich Stadial 1
- A similar amplification during the Younger Dryas is not observed, suggesting mean state may mediate millennial-scale ENSO variability

Supporting Information:

Supporting Information may be found in the online version of this article.

Correspondence to:

R. H. Glaubke,
rglaubke@marine.rutgers.edu

Citation:

Glaubke, R. H., Schmidt, M. W., Hertzberg, J. E., Ward, L. G., Marcantonio, F., Schimmenti, D., & Thirumalai, K. (2024). An inconsistent ENSO response to Northern Hemisphere stadials over the last deglaciation. *Geophysical Research Letters*, *51*, e2023GL107634. https://doi.org/10.1029/2023GL107634

Received 1 DEC 2023
Accepted 24 MAY 2024

Abstract The dynamics shaping the El Niño-Southern Oscillation's (ENSO) response to present and future climate change remain unclear, partly due to limited paleo-ENSO records spanning past abrupt climate events. Here, we measure Mg/Ca ratios on individual foraminifera to reconstruct east Pacific subsurface temperature variability, a proxy for ENSO variability, across the last 25,000 years, including the millennial-scale events of the last deglaciation. Combining these data with proxy system model output reveals divergent ENSO responses to Northern Hemisphere stadials: enhanced variability during Heinrich Stadial 1 (H1) and reduced variability during the Younger Dryas (YD), relative to the Holocene. H1 ENSO likely intensified through meltwater-induced changes to ocean/atmospheric circulation, a response observed in models, but the lack of a similar response during the YD challenges model simulations. We suggest the tropical Pacific mean state during H1 primed ENSO for larger fluctuations under meltwater forcing, whereas the YD mean state likely buffered against it.

Plain Language Summary The El Niño-Southern Oscillation (ENSO) is one of the planet's largest and most influential recurring climate patterns. The fluctuation between warm (El Niño) and cold events (La Niña) every several years has a substantial impact on global weather patterns that carry important socioeconomic consequences. How the frequency and severity of ENSO events may change in response to present and future climate change is largely uncertain, although lessons from past abrupt climate events can help inform our projections of future ENSO. To that end, we analyzed the chemical composition of small, individual zooplankton shells buried in marine sediments to reconstruct "snapshots" of subsurface temperature variability in the eastern Pacific, a feature closely linked to ENSO, over the last 25,000 years. During this time, two abrupt climate events induced by melting glacial ice ("Heinrich Stadial 1" and the "Younger Dryas") were characterized by different ENSO responses (stronger and weaker, respectively). We suggest that the average climate conditions in the tropical Pacific (temperature, wind strength, etc.) played an important role by either priming the ENSO system for disruption by meltwater (Heinrich Stadial 1) or buffering against it (Younger Dryas).

1. Introduction

As the Earth system's largest source of interannual climate variability, the El Niño-Southern Oscillation (ENSO) exerts a considerable influence over global temperature and precipitation patterns that have a profound impact on people's lives, livelihoods, and health (Glantz, 2001; IPCC, 2021). In recent decades, the socioeconomic effects of three record-breaking El Niño events (1982/83, 1997/98, and 2015/16) have emphasized the need to better understand ENSO's sensitivity to global climate change and its potential response to future warming. Projections of future ENSO amplitude and frequency—collectively referred to as ENSO variability—are not well constrained (Collins et al., 2010; IPCC, 2021), underscoring the need for a more detailed understanding of how abrupt climate change influences the processes and feedbacks that govern ENSO behavior. The instrumental record, while sufficient to improve near-term ENSO forecasts (L'Heureux et al., 2020), is too brief to fully constrain long-term ENSO dynamics. Instead, a network of paleoclimate observations is required, particularly across periods of naturally abrupt climate change, to broaden our perspective of ENSO variability and its relationship to mean tropical climate (Emile-Geay et al., 2020).

Reconstructions of past ENSO variability from coral skeletons (Cobb et al., 2013; Emile-Geay et al., 2016; Grothe et al., 2020; McGregor & Gagan, 2004; Tudhope et al., 2001), marine bivalves (Carré et al., 2014, 2021; Emile-Geay et al., 2016), lake sediments (Conroy et al., 2008; Moy et al., 2002; Rodbell et al., 1999), and marine

sediment cores (Ford et al., 2015; Koutavas et al., 2006; Koutavas & Joanides, 2012; Leduc et al., 2009; Rein et al., 2005; Rustic et al., 2020; Sadekov et al., 2013; White et al., 2018) have been instrumental in constraining ENSO behavior over the Holocene and the LGM. However, there is a scarcity of ENSO-resolvable records spanning the last deglaciation—a period of global warming characterized by millennial-scale fluctuations in surface temperatures (Shakun et al., 2012), atmospheric CO_2 concentrations (Bereiter et al., 2015; Petit et al., 1999), ice sheet extent (Bentley et al., 2010; Carlson et al., 2008), and oceanic and atmospheric circulation (Broccoli et al., 2006; McManus et al., 2004; Reimi & Marcantonio, 2016; Schmidt et al., 2012; Them et al., 2015). There is little agreement as to how ENSO responded to deglacial climate change among the few paleo-ENSO records available from this interval. It is difficult to determine whether these disagreements are a true reflection of ENSO history or arise due to conflicting environmental signals and other sources of uncertainty obscuring the ENSO signal preserved in the sedimentary record (see Supporting Information S1). Without additional data and a standardized method for comprehensively treating proxy uncertainty, our knowledge of deglacial ENSO remains thin (Lu et al., 2018).

At present, our best understanding of deglacial ENSO dynamics comes from paleoclimate modeling. Sensitivity experiments from the transient climate simulation TraCE-21ka (hereafter TRACE) suggest ENSO underwent substantial millennial-scale changes across the last deglaciation in response to variations in meltwater discharge (Z. Liu et al., 2014). In these simulations, a meltwater-induced disruption of oceanic and atmospheric circulation weakens the equatorial annual cycle in the eastern equatorial Pacific (EEP), relaxing its phase-locked relationship with ENSO which enhances variability. Similar findings from freshwater hosing experiments across multiple fully coupled general circulation models (Braconnot et al., 2012; Luan et al., 2015; Merkel et al., 2010; Timmermann, Lorenz, et al., 2007; Timmermann, Okumura, et al., 2007) indicate a prominent role for remote meltwater forcing in shaping deglacial ENSO variability. However, improving paleodata coverage across the last deglaciation is necessary to evaluate the validity of this simulated meltwater influence.

To that end, we present new records of subsurface temperature variability from high-resolution piston core MV1014-02-17JC (0.18°S, 85.87°W, 2,846 m; hereafter 17JC) and nearby multicore MV1014-02-09MC (0.69°S, 85.33°W; 2,452 m; hereafter 09MC) in the heart of the EEP (Figure 1a). El Niño and La Niña events strongly modulate the depth of the thermocline in this region (Fiedler & Talley, 2006), and so reconstructions of subsurface temperature variability have been used to infer ENSO variability in the past (Ford et al., 2015; Leduc et al., 2009; Thirumalai et al., 2013). We analyze the single-shell trace element composition of the thermocline-dwelling foraminifera *Neogloboquadrina dutertrei* to reconstruct the distribution of Mg/Ca-derived paleotemperatures from several targeted time horizons spanning the last 25,000 years (25 ka). The relatively high sedimentation rate in 17JC (~18 cm/kyr) allows us to resolve the millennial-scale events of the last deglaciation more clearly than has been achieved by prior single-shell Mg/Ca reconstructions (Sadekov et al., 2013; White et al., 2018). We support our paleo-ENSO reconstruction with simulations from the new Quantile Analysis of Temperature using Individual Foraminiferal Analyses (QUANTIFA) proxy system model (Glaubke et al., 2021), which provides a comprehensive framework for constraining uncertainties intrinsic to individual foraminiferal analyses (IFA), as well as robust tools for deconvolving the ENSO signal from other sources of paleotemperature variability. Our findings offer new insights into deglacial ENSO behavior and provide crucial observational context for ENSO simulations (Lu et al., 2018).

2. Material and Methods

2.1. Age Model

The age model for 17JC is based on 18 published radiocarbon dates on pooled specimens of *N. dutertrei* (>250 μm) (Table S1 in Supporting Information S1; Loveley et al., 2017; Schimmenti et al., 2022). Radiocarbon ages were converted to calendar years using the Bayesian statistical package "rbacon" for R and the Marine20 calibration data set with an age correction of 500 years (Blaauw & Christen, 2011). For the core-top of 09MC, one radiocarbon date on a pooled sample of *N. dutertrei* (>250 μm) was calibrated using the latest version of the Calib software (v8.2) and the Marine20 data set, yielding a core-top age of 1.97 ± 0.16 ka. The average sedimentation rate for 17JC is ~18 cm kyr^{-1} based on linear interpolation between radiocarbon dates (Figure S1 in Supporting Information S1), resulting in a nominal sampling resolution of ~55 years cm^{-1}. Allowing for a bioturbation depth of 5–10 cm (Solan et al., 2019) and assuming a constant sedimentation rate, a simple biodiffusion model (Berger

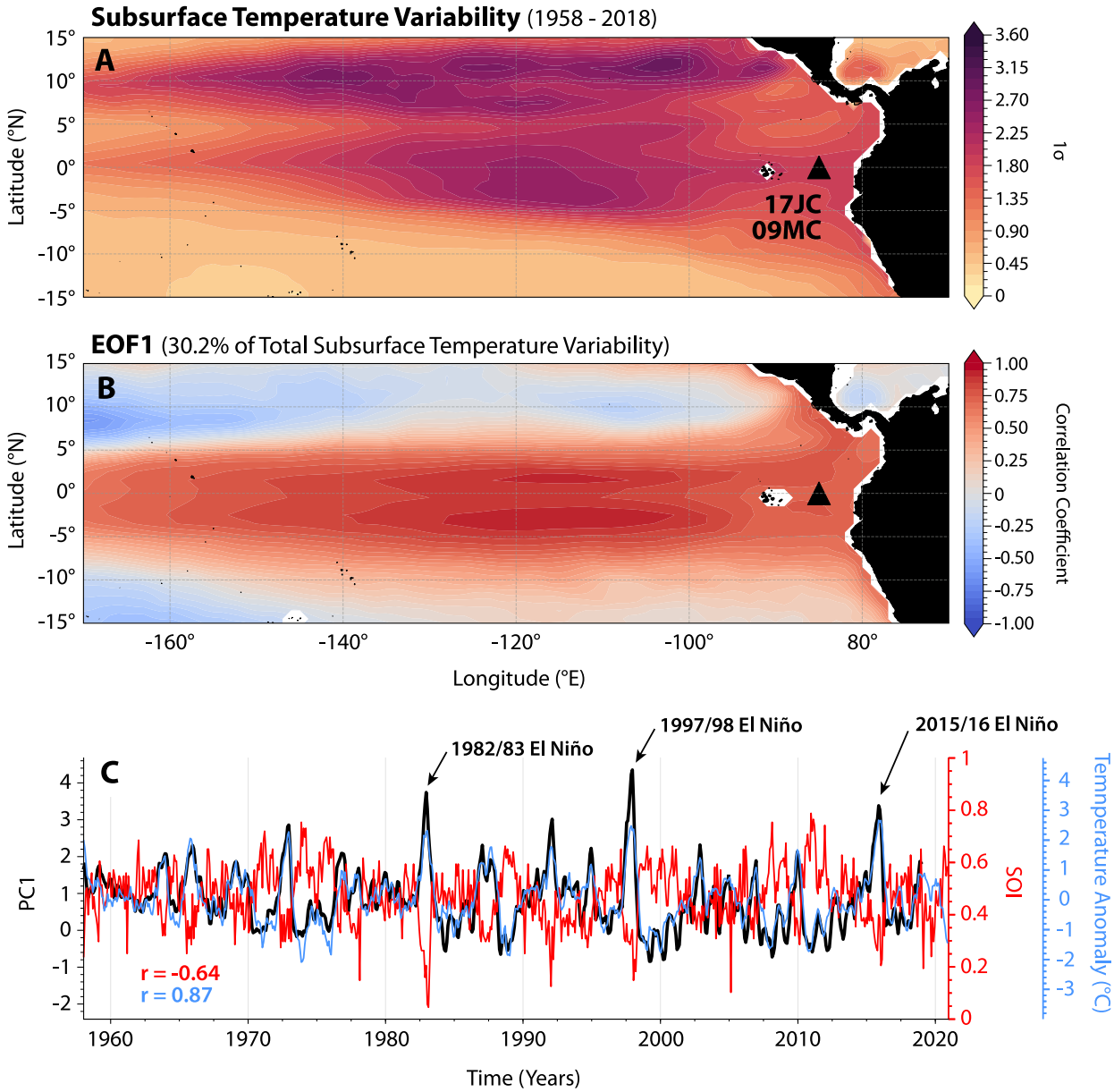

Figure 1. ENSO's contribution to subsurface temperature variability in the eastern equatorial Pacific (EEP). (a) Subsurface temperature variability within the EEP between 40 and 120 m depth (data from Ocean Reanalysis System 5; Zuo et al., 2019). The location of cores 17JC and 09MC are designated by the black triangle. (b) The pattern of the first empirical mode (EOF1), which strongly resembles the spatial footprint of an East Pacific El Niño. (c) The temporal variability of principal component 1 (PC1; black) and its correlation to both atmospheric (Southern Oscillation Index, or SOI; red) and oceanic indices of ENSO (Niño 3.4 sea surface temperature anomaly; blue). The record-breaking El Niño events of the last few decades are denoted in the time series.

& Heath, 1968) suggests ~85%–94% of randomly selected foraminifera from a single interval would have been deposited within ±550 years of the sample's nominal age.

Previously published down-core records from 17JC can be found in their respective publications (Loveley et al., 2017; Schimmenti et al., 2022). Isotopic stratigraphy can be found in Supporting Information S1.

2.2. Individual Foraminiferal Analyses

At least 70 individual *N. dutertrei* (450–500 μm) were collected from seven discrete intervals in 17JC and 09MC, a sample size that has been shown to sufficiently capture population statistics (Thirumalai et al., 2013). The selected intervals span the late Holocene (LH; 1.97 ka), the early Holocene (EH1 and EH2; 8.49 and 10.1 ka,

respectively), the YD (12.3 ka), the Bølling-Allerød (BA; 13.4 ka), H1 (14.9 ka), and the LGM (19.7 ka) (Table S2 in Supporting Information S1). Whole *N. dutertrei* shells were loaded into micro-centrifuge vials, immersed in ultra-pure water, and gently crushed. Samples were sonicated for 15–20 s in ultra-pure water (5x) and methanol (2x) to remove clays, treated with a hot oxidizing solution to eliminate remnant organic matter, centrifuged at 7,000 rpm for 60 s, and transferred into new acid-leached vials. The reductive step and the final weak nitric acid leach were eliminated to minimize sample loss. All clean work was conducted in laminar flow benches under trace metal clean conditions.

Samples were dissolved in 2% nitric acid and run on an Element XR HR-ICP-MS at Old Dominion University. Long-term analytical precision (1σ) across all runs was 2.38%, 1.18%, and 0.81% for three consistency standards with Mg/Ca ratios of 0.803, 1.419, and 2.034 mmol/mol, respectively ($n = 20$). Al/Ca, Fe/Ca, and Mn/Ca ratios were monitored as indicators of cleaning efficacy, while ^{43}Ca intensities were viewed as an indicator of sample size. Approximately 15%–25% of individuals per time slice returned high Al/Ca, Fe/Ca, or Mn/Ca ratios (>150 μmol/mol) or low percent recovery (<15%) and were rejected. No systemic relationship was observed between Mg/Ca and our cleaning indicators (Figure S3 in Supporting Information S1). Mg/Ca ratios were translated to subsurface temperatures using a species-specific *N. dutertrei* equation developed in the east Pacific with a static dissolution correction term included as a function of core depth (Dekens et al., 2002).

2.3. Data Analysis and Proxy System Modeling

To assess differences in structure between our reconstructed paleotemperature distributions, we use quantile-quantile analysis, a non-parametric method of comparing distribution data that has become the standard for IFA studies (Ford et al., 2015; Thirumalai et al., 2019; White et al., 2018). Quantile plots conveniently capture differences in spread, skew, and shape between two distributions in one plot; however, exactly how these differences translate to changes in high-frequency climate variability is difficult to determine from the plots alone.

We therefore compare the structure of the quantile-quantile plots against idealized results from a suite of hypothetical, forward-modeled climate scenarios simulated by the proxy system model QUANTIFA (Glaubke et al., 2021). In these statistical experiments, the ENSO (amplitude and frequency) and annual cycle signals in reanalysis ocean temperature data from our location are systematically modified from their modern climatologies (from −100% to +100% at 10% increments) and forward modeled into Mg/Ca ratios to create pseudoproxy records of altered climate variability ($n = 440$; see Supporting Information S1). These records are repeatedly subsampled ($n = 10{,}000$) and compared to populations from a pseudoproxy record of modern climate variability —an exercise analogous to our IFA analysis—to generate characteristic quantile-quantile structures describing the data's expected response to altered climate variability. These simulations also provide 1σ uncertainties representing the full propagation of analytical, calibration, and sampling errors (Glaubke et al., 2021), as well as uncertainty in the living depth and growth season of *N. dutertrei* (see Supporting Information S1). We align our results against these simulations to determine the set of hypothetical climate scenarios that best match our observations, which are marked as “hot spots” in a series of data-model consistency maps (see Figure S4 in Supporting Information S1 for theoretical examples).

For more information on QUANTIFA's statistical framework, model parameterizations, and uncertainties, see Glaubke (2023) and the Supporting Information S1.

3. Climate Controls Over IFA Distributional Shape

Multiple sources of climatological and ecological variability are incorporated into the IFA-derived paleotemperature distributions. Layered on top of this amalgamized environmental signal is uncertainty associated with the physical recovery and analysis of individual foraminifera. Before using IFA to reconstruct ENSO, we must first establish that the ENSO signal dominates ocean temperature variability in the region and that it stands out in local IFA populations amidst the “noise” of other sources of variability.

In the EEP, upper ocean temperature variability is primarily driven by the annual cycle and ENSO phase changes (Fiedler & Talley, 2006). Both signals contribute equally to the variability observed in the surface ocean; however, the influence of the annual cycle is more muted at depth (Fiedler & Talley, 2006). In the subsurface, where *N. dutertrei* generally reside (76 ± 41 m) (Ford et al., 2018), a principal component analysis of Ocean Reanalysis System 5 (ORA-S5) temperatures identifies ENSO as the dominant component of regional

spatiotemporal variability (Figure 1). This subsurface ENSO fingerprint can be attributed to migrations of the regional thermocline during ENSO events, which mooring arrays and isolated hydrographic casts reveal induces large temperature anomalies in the EEP subsurface (Figure S5 in Supporting Information S1).

We use the idealized results from QUANTIFA to determine how clearly this ENSO-dominated signal is preserved in reconstructed paleotemperature distributions at our core site, as well as how sensitive they are to changes in ENSO variability and the annual cycle (Figure S6 in Supporting Information S1). The results suggest the strength of the ENSO signal is more than twice that of the annual cycle (2.25x). The mean response of simulated quantiles to changing ENSO variability (±0.58°C; 1σ) is more readily detected than changes in the annual cycle (±0.27°C; 1σ) given an average baseline uncertainty of ±0.23°C attributable to foraminiferal ecology, random sampling, and both analytical and calibration error. As such, ENSO variability is the most prominent signal shaping the paleotemperature distributions preserved by local *N. dutertrei*, whereas the influence of the annual cycle is largely negligible with the small exception of a narrow range of hypothetical climate states. When ENSO variability is reduced (<−40%), a stronger annual cycle (>+50%) can compensate for the resulting decrease in subsurface temperature variability to resemble variability in the modern ocean, a scenario that is difficult to resolve by our methodology (Figure S6 in Supporting Information S1).

This interpretive framework assumes stationarity in the EEP's sensitivity to ENSO-related temperature anomalies through time. Given evidence from the Holocene that different ENSO "flavors" have distinct temperature expressions (Carlo et al., 2023; Carré et al., 2014; Karamperidou et al., 2015), our final conclusions are necessarily limited to the East Pacific variety of ENSO. We also assume that *N. dutertei*'s ecological preferences in space (depth habitat) and time (seasonal productivity) remained similar across the deglaciation relative to when and where ENSO anomalies are expressed in the EEP. Nevertheless, our statistical analysis demonstrates that the *N. dutertrei* at our core site offer a robust representation of interannual temperature variations in the EEP, strongly modulated by past ENSO variability. We therefore infer a discrete history of ENSO variability over the last 25 ka by evaluating differences in the shape and structure of these paleotemperature distributions down-core.

4. ENSO Variability Over the Last 25,000 Years

Down-core paleotemperature distributions from 17JC are compared to the LH core-top distribution of 09MC in Figure 2 (raw data can be found in Figure S7 of Supporting Information S1). Our results reveal regions of the distributions, typically in both tails and in the cold spectrum of the distributional interior, where quantiles deviate from a 1:1 equilibrium line beyond their 90% confidence envelopes (Figure 2; white circles). We observe a pattern where the coldest (warmest) quantiles plot above (below) the 1:1 line in nearly all comparisons, an indication of reduced paleotemperature variability. However, the comparison with H1 is different, with significant quantiles in the interior deviating in the opposite direction (Figure 2e).

When compared to the results simulated by QUANTIFA, nearly all the maps associated with our core-top comparisons show regions of data-model consistency concentrated in the third and, to a lesser extent, second quadrants of the consistency map (Figures 3a–3d and 3f). These quadrants represent modeled scenarios of reduced ENSO variability. The “hot spots” do not extend completely into quadrant two because it represents scenarios where ENSO is reduced and the annual cycle is amplified which, as detailed above, our IFA populations have difficulty resolving (Figure S6 in Supporting Information S1). Nevertheless, the clustering of data-model consistency on the left-hand side of the maps strongly implies that ENSO variability was diminished for nearly every interval relative to the LH. The sole exception to this pattern is H1 (Figure 3e). Here, we find that data-model consistency is confined to quadrants one and four, a region representing scenarios of enhanced ENSO variability. Our data therefore suggest that ENSO variability during H1 was stronger and/or more frequent than any other time period considered here.

To visualize the evolution of inferred ENSO variability across the last deglaciation, we compute the barycenter (or weighted geometric center) of the data-model consistency maps (Figure 3g), the x-coordinate of which provides a rough estimate of ENSO change (%) relative to the LH for each of our sampled intervals (Figure 4a). The barycenters emphasize the substantial increase in ENSO-related interannual variability during H1 (+31%) relative to the LH. The LGM, BA, and both EH intervals report similar reductions (∼−43% to −46%) relative to the LH, and the YD reported the lowest inferred variability (−56%). We emphasize that these barycenters are used illustratively, rather than to provide empirical estimates of past ENSO variability. Nevertheless, they offer a discrete history of ENSO evolution over the last 25 ka, beginning with a sharp intensification at the end of the

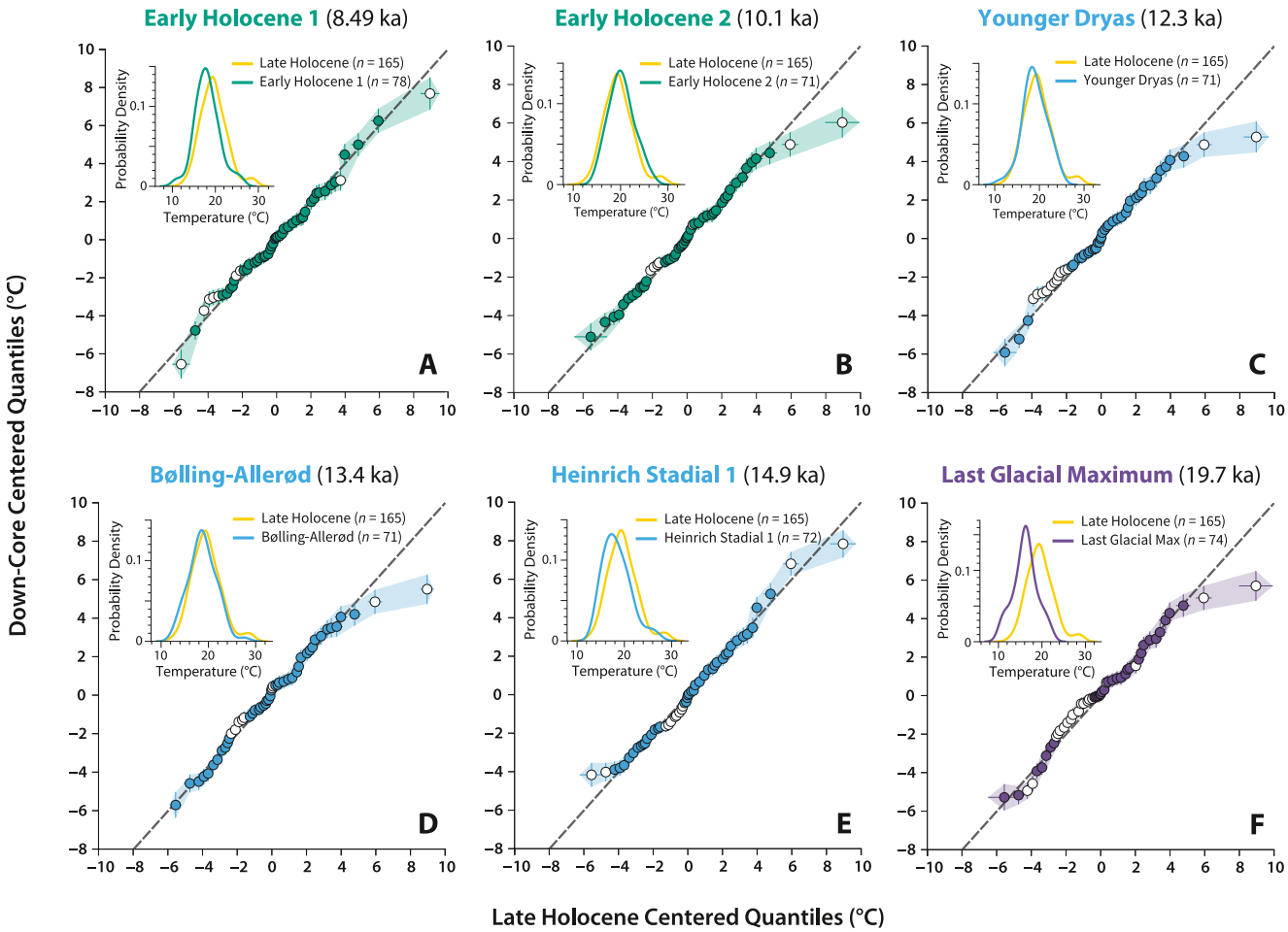

Figure 2. Quantile-quantile plots of individual foraminiferal analyses population comparisons. Plots reveal significant differences between the (a and b) early Holocene, (c–e) deglacial, and (f) LGM intervals relative to the LH. White quantiles significantly deviate from the 1:1 line with 90% confidence. Envelopes represent the 90% confidence region incorporating ecological, sampling, analytical, and calibration error in both populations. Inset shows Gaussian kernel density estimates of each paleotemperature distribution to illustrate differences in the shape of each distribution.

LGM, a decline in variability throughout the deglaciation, and an increase in variability across the Holocene (Figure 4a). Notably, this record highlights an intriguing inconsistency in the ENSO response to Northern Hemisphere stadials: strong variability during H1 and weak variability during the YD.

5. ENSO Intensification During Heinrich Stadial 1

Considering that all other sampling intervals show reduced variability relative to the LH, the pronounced increase in ENSO-related variability during H1 is striking. In TRACE, a comparable response is observed in both the full forcing simulation (Figure 4b; red line) and a single-forcing meltwater experiment (Figure 4b; blue line). The authors attribute this ENSO behavior to reorganizations of oceanic and atmospheric circulation that modify ENSO through its phase locking with the EEP annual cycle (Z. Liu et al., 2014)—a mechanism known as "frequency entrainment" (Z. Liu et al., 2014). In many (An & Choi, 2014; Z. Liu et al., 2014; Timmermann, Lorenz, et al., 2007)—although not all (Braconnot et al., 2012; Carré et al., 2021; Salau et al., 2012)—climate models, ENSO can relinquish its natural oscillatory mode to acquire a more annual frequency when the annual cycle is sufficiently strong, leading to a decrease in interannual variability (Chang et al., 1994, 1995; Z. Liu, 2002). Conversely, weakening the annual cycle relaxes this phase locking, allowing for enhanced ENSO-driven interannual variability. In TRACE, the influx of freshwater into the North Atlantic during H1 weakens the strength of the Atlantic Meridional Overturning Circulation (AMOC), which in turn forces a southward shift in the mean position of the Intertropical Convergence Zone (ITCZ). The more southerly ITCZ enhances trade

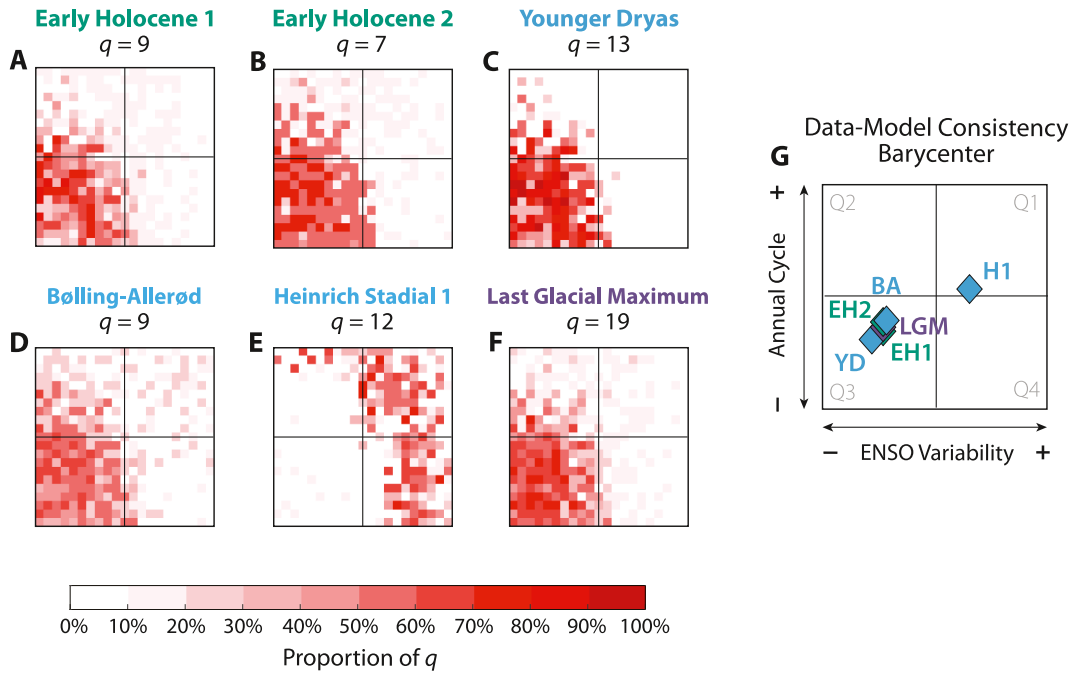

Figure 3. Maps of data-model consistency between the observed results from 17JC and forward-modeled results simulated by QUANTIFA. (a–f) Consistency maps reporting the proportion of significant quantiles (white circles identified in Figure 2) that exhibit good data-model agreement (i.e., are within 1σ) with those same quantiles in each hypothetical climate scenario. The total number of significant quantiles are labeled as "q" above the consistency maps. The provenance of the data-model consistency "hot spots" is used to diagnose past climate variability relative to the LH, as illustrated in panel (g). (g) Location of the barycenters for each data-model consistency map.

wind strength over the EEP, creating a more symmetrical north-south temperature gradient that dampens the seasonality of surface temperatures entraining ENSO to the annual cycle (Lu et al., 2016; Timmermann, Okumura, et al., 2007). Barring influences from other local or remote forcings (Z. Liu et al., 2014), the weakening of the annual cycle allows for enhanced ENSO variability during H1.

Our data, taken together with existing records, are potentially consistent with the frequency entrainment hypothesis during H1. During this period, proxy records from the Bermuda Rise (McManus et al., 2004) (Figure 4c) provide evidence for a substantial slowdown of the AMOC and a compilation of speleothems from nearby Ecuador (Mosblech et al., 2012) (Figure 4d) indicate an associated southward displacement of the ITCZ, both of which would serve to weaken the annual cycle of the tropical Pacific (Z. Liu et al., 2014). Our IFA observations indicate significantly enhanced subsurface temperature variability during this interval, which our proxy system model attributes to ENSO-related interannual temperature variations (Figure 3). These results generally agree with findings from a nearby paleo-ENSO reconstruction based on the same foraminiferal species (Sadekov et al., 2013) and support an inferred increase in H1 ENSO variability relative to glacial conditions reported in another (Leduc et al., 2009). This correspondence may suggest an emerging consensus over increased ENSO variability during H1, despite disagreements over its magnitude relative to the Late Holocene (see Supporting Information S1). However, the lowered sensitivity of our proxy environment to changes in the annual cycle (Figure S6 in Supporting Information S1) precludes the robust identification of a weaker annual cycle during H1. We suggest that future studies in properly targeted proxy environments could be paired with our data to further establish the validity of the frequency entrainment hypothesis.

Unlike H1, intensification of ENSO does not occur during the YD, another millennial-scale climate event associated with significant meltwater influx to the North Atlantic. In TRACE, meltwater forcing drives a peak in ENSO variability (Figure 4b; blue line) that appears more subdued in the full-forcing simulation (Figure 4b; red line) (Z. Liu et al., 2014; Lu et al., 2016). Our reconstruction shows the YD as the least variable interval of the last 25 ka, suggesting forcings other than meltwater may be at play.

10.1029/2023GL107634

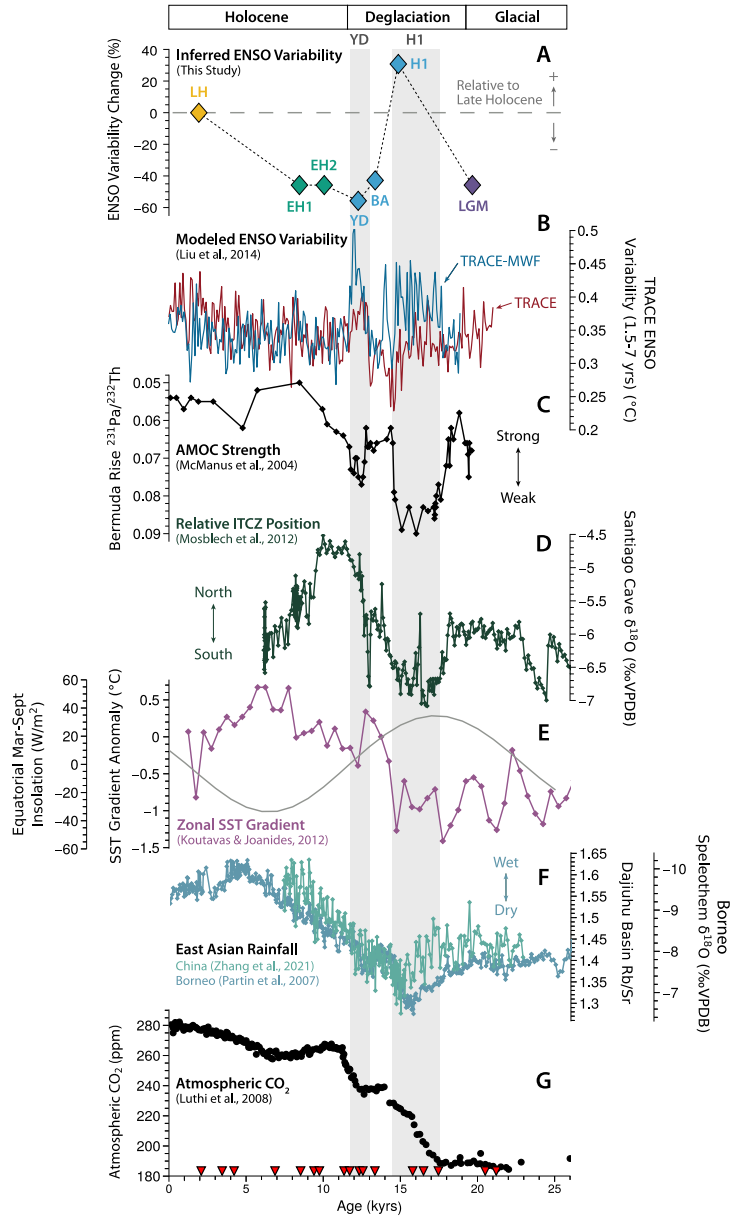

Figure 4. ENSO variability and its relationship to background climate conditions over the last deglaciation. (a) ENSO-related interannual temperature variability estimated from the *x*-coordinate of the data-model consistency barycenters. (b) Simulated ENSO variability from the full TRACE simulation (red) and meltwater forcing experiment (TRACE-MWF) (blue; Liu et al., 2014) reported as sea surface temperature variability in the 1.5–7 years band from the Niño3.4 region. (c) $^{231}Pa/^{230}Th$ ratios from core GGC5 on the Bermuda Rise, a proxy for Atlantic Meridional Overturning Circulation (AMOC) intensity (McManus et al., 2004). Lower $^{231}Pa/^{230}Th$ is interpreted as enhanced AMOC transport, and vice versa. (d) Composite speleothem $\delta^{18}O$ from Santiago Cave in Ecuador nearby our core site (3°1′S, 78°8′W), a record of shifts in the relative position of the Intertropical Convergence Zone (ITCZ) (Mosblech et al., 2012). More depleted $\delta^{18}O$ values are indicative of increased rainfall intensity brought on by a more southerly position of the ITCZ, and vice versa. (e) A reconstruction of the zonal SST gradient across the tropical Pacific (purple; Koutavas & Joanides, 2012) and the difference between March and September insolation at the equator (gray). (f) Two records of east Asian hydroclimate in key ENSO-sensitive regions: Rb/Sr ratios in lake core LC1 from Dajiuhu Basin, central China (teal; Zhang et al., 2021) and a composite speleothem $\delta^{18}O$ record from Borneo (slate blue; Partin et al., 2007). (g) Atmospheric carbon dioxide concentrations as recorded in air bubbles trapped within the EPICA Dome C ice core from Antarctica (Lüthi et al., 2008). The timing of the Younger Dryas and H1 is represented by vertical gray bars. Radiocarbon dates from 17JC are indicated by the red triangles along the *x*-axis.

6. An Inconsistent ENSO Response to Stadial Events: A Role for the Tropical Pacific Mean State?

We propose that the influence of remote meltwater forcing on ENSO could be a function of the mean climate state across the tropical Pacific—namely, whether it is conducive to the initiation and propagation of ENSO events. During H1, insolation at the equator was at a maximum in March and a minimum in September, producing differential heating across the Pacific that weakened the mean annual east-west surface temperature gradient (Koutavas & Joanides, 2012) (Figure 4e). Consequently, the intensity of the Walker Circulation could have diminished, weakening surface wind stress that would normally serve as a barrier against the eastward propagation of warm surface waters at the onset of El Niño (Clement et al., 2000). This mean state configuration of the upper ocean/atmosphere could have preconditioned the tropical Pacific for the development of stronger, more frequent, and/or more persistent El Niño events (Clement et al., 1996). Indeed, the enhanced ENSO variability in our H1 interval coincides with other proxy indications of a diminished Walker Circulation, including a minimum mean annual zonal temperature gradient (Koutavas & Joanides, 2012) (Figure 4e) and drought-like conditions in ENSO-sensitive regions such as Borneo (Partin et al., 2007) and central China (Zhang et al., 2021) (Figure 4f), reinforcing this interpretation.

Following H1, the timing of maximum insolation on the equator began to shift from March toward September, yielding a pattern of warming that increasingly reinforced the mean annual zonal temperature gradient across the tropical Pacific (Figure 4e). In response, the Walker Circulation and the associated surface wind stress likely strengthened, establishing background climate conditions more resistant to the development of ENSO events. During the YD, such a mean state may have fortified the ENSO system against the disruption brought on from meltwater and associated forcings.

The tropical Pacific mean state may have worked in tandem with other features of the global background climate to modulate the influence of meltwater forcing over ENSO. For example, the more southerly mean position of the ITCZ during H1, established by an extensive Laurentide ice sheet (Chiang & Bitz, 2005), may have made it more likely for migrations associated with a weakened AMOC to influence the tropical Pacific ocean-atmosphere system. As the ice retreated across the deglaciation, orbital precession became a more dominant influence over ITCZ position, helping to buffer its migratory response to AMOC weakening (Mosblech et al., 2012). The brevity of the YD event in the Santiago Cave speleothem composite from Ecuador (Figure 4d) suggests the state of this ice sheet/insolation force balance may have resulted in an ITCZ migration too rapid to sustain the enhanced ENSO variability simulated by TRACE. Additionally, an abrupt increase in atmospheric CO_2 concentrations during the YD (Figure 4g) could have diminished ENSO-related variability (Z. Liu et al., 2014). The results from TRACE suggest CO_2 was likely insufficient to counteract a meltwater-induced increase in variability during the YD (Z. Liu et al., 2014). However, simulations from ultra-high-resolution climate models suggest rising CO_2 concentrations can impact mesoscale processes in the atmosphere that dampen ENSO-related variability more effectively than observed in lower resolution simulations (Wengel et al., 2021). These dynamics could have been more prominent during the YD than H1 owing to its higher background CO_2 levels, although simulations of past climate using these ultra-high-resolution models are required to confirm such mechanisms.

7. Conclusions

Taken together, our new paleo-ENSO record provides crucial observational context for the consistent link between ENSO and meltwater forcing reproduced in paleo-ENSO model simulations (Braconnot et al., 2012; Z. Liu et al., 2014; Timmermann, Lorenz, et al., 2007; Timmermann, Okumura, et al., 2007). When considered alongside other published data, our data suggest ENSO's response to meltwater forcing may depend on how primed the tropical Pacific is to the development of frequent and/or extreme ENSO events. While not a perfect analog for the future, this hypothesis is relevant for understanding future ENSO variability. Climate models suggest the zonal temperature gradient of the tropical Pacific and trade wind strength may weaken under greenhouse warming (Collins et al., 2010; Lee et al., 2022), and modern observations warn of a weakening AMOC in response to Greenland ice melt (Boers, 2021; Caesar et al., 2021; Rahmstorf et al., 2015; Yang et al., 2016). The combined influence of these background climate conditions during H1 might suggest enhanced ENSO variability in the near future (Cai et al., 2015; W. Liu et al., 2023). In this context, modeling experiments testing the influence of meltwater forcing under different mean state configurations are clearly needed to clarify ENSO dynamics both during the deglaciation and in the future.

Conflict of Interest

The authors declare no conflicts of interest relevant to this study.

Data Availability Statement

All single-shell trace element data presented in this manuscript are available through the NOAA National Centers for Environmental Information at Glaubke et al. (2024). The QUANTIFA model can be accessed through Zenodo at Glaubke (2023).

Acknowledgments
The authors would like to thank the three anonymous reviewers whose comments improved the quality of our manuscript. The authors would also like to acknowledge Tom Marchitto for sharing cleaning protocols for individual foraminifera, Zhengyu Liu and Zhengyao Lu for providing TRACE output, and Bettina Sohst for her limitless talent and patience on the ICP-MS. This project was supported by funds from the National Science Foundation awarded to M.W.S. (OCE-1701380) and K.T. (MGG-1903482) and from Old Dominion University's College of Sciences (Neil and Susan Kelly Endowed Scholarship) awarded to R.H.G.

References

An, S.-I., & Choi, J. (2014). Mid-Holocene tropical Pacific climate state, annual cycle, and ENSO in PMIP2 and PMIP3. *Climate Dynamics*, *43*(3–4), 957–970. https://doi.org/10.1007/s00382-013-1880-z

Bentley, M. J., Fogwill, C. J., Brocq, A. M. L., Hubbard, A. L., Sugden, D. E., Dunai, T. J., & Freeman, S. P. H. T. (2010). Deglacial history of the West Antarctic Ice Sheet in the Weddell Sea embayment: Constraints on past ice volume change. *Geology*, *38*(5), 411–414. https://doi.org/10.1130/g30754.1

Bereiter, B., Eggleston, S., Schmitt, J., Nehrbass-Ahles, C., Stocker, T. F., Fischer, H., et al. (2015). Revision of the EPICA Dome C CO_2 record from 800 to 600 kyr before present. *Geophysical Research Letters*, *42*(2), 542–549. https://doi.org/10.1002/2014gl061957

Berger, W. H., & Heath, G. R. (1968). Vertical mixing in pelagic sediments. *Journal of Marine Research*, *26*(2), 1122.

Blaauw, M., & Christen, J. A. (2011). Flexible paleoclimate age-depth models using an autoregressive gamma process. *Bayesian Analysis*, *6*(3), 457–474. https://doi.org/10.1214/11-ba618

Boers, N. (2021). Observation-based early-warning signals for a collapse of the Atlantic Meridional Overturning Circulation. *Nature Climate Change*, *11*(8), 680–688. https://doi.org/10.1038/s41558-021-01097-4

Braconnot, P., Luan, Y., Brewer, S., & Zheng, W. (2012). Impact of Earth's orbit and freshwater fluxes on Holocene climate mean seasonal cycle and ENSO characteristics. *Climate Dynamics*, *38*(5–6), 1081–1092. https://doi.org/10.1007/s00382-011-1029-x

Broccoli, A. J., Dahl, K. A., & Stouffer, R. J. (2006). Response of the ITCZ to Northern Hemisphere cooling. *Geophysical Research Letters*, *33*(1), L01702. https://doi.org/10.1029/2005gl024546

Caesar, L., McCarthy, G. D., Thornalley, D. J. R., Cahill, N., & Rahmstorf, S. (2021). Current Atlantic Meridional Overturning Circulation weakest in last millennium. *Nature Geoscience*, *14*(3), 118–120. https://doi.org/10.1038/s41561-021-00699-z

Cai, W., Santoso, A., Wang, G., Yeh, S.-W., An, S.-I., Cobb, K. M., et al. (2015). ENSO and greenhouse warming. *Nature Climate Change*, *5*(9), 849–859. https://doi.org/10.1038/nclimate2743

Carlo, I. A. D., Braconnot, P., Carré, M., Elliot, M., & Marti, O. (2023). Different methods in Assessing El Niño flavors lead to opposite results. *Geophysical Research Letters*, *50*(15), e2023GL104558. https://doi.org/10.1029/2023gl104558

Carlson, A. E., LeGrande, A. N., Oppo, D. W., Came, R. E., Schmidt, G. A., Anslow, F. S., et al. (2008). Rapid early Holocene deglaciation of the Laurentide ice sheet. *Nature Geoscience*, *1*(9), 620–624. https://doi.org/10.1038/ngeo285

Carré, M., Braconnot, P., Elliot, M., d'Agostino, R., Schurer, A., Shi, X., et al. (2021). High-resolution marine data and transient simulations support orbital forcing of ENSO amplitude since the mid-Holocene. *Quaternary Science Reviews*, *268*, 107125. https://doi.org/10.1016/j.quascirev.2021.107125

Carré, M., Sachs, J. P., Purca, S., Schauer, A. J., Braconnot, P., Falcón, R. A., et al. (2014). Holocene history of ENSO variance and asymmetry in the eastern tropical Pacific. *Science*, *345*(6200), 1045–1048. https://doi.org/10.1126/science.1252220

Chang, P., Ji, L., Wang, B., & Li, T. (1995). Interactions between the seasonal cycle and El Niño-Southern Oscillation in an intermediate coupled ocean-atmosphere model. *Journal of the Atmospheric Sciences*, *52*(13), 2353–2372. https://doi.org/10.1175/1520-0469(1995)052<;2353:ibtsca>2.0.co;2

Chang, P., Wang, B., Li, T., & Ji, L. (1994). Interactions between the seasonal cycle and the Southern Oscillation - Frequency entrainment and chaos in a coupled ocean-atmosphere model. *Geophysical Research Letters*, *21*(25), 2817–2820. https://doi.org/10.1029/94gl02759

Chiang, J. C. H., & Bitz, C. M. (2005). Influence of high latitude ice cover on the marine Intertropical Convergence Zone. *Climate Dynamics*, *25*(5), 477–496. https://doi.org/10.1007/s00382-005-0040-5

Clement, A. C., Seager, R., & Cane, M. A. (2000). Suppression of El Niño during the Mid-Holocene by changes in the Earth's orbit. *Paleoceanography*, *15*(6), 731–737. https://doi.org/10.1029/1999pa000466

Clement, A. C., Seager, R., Cane, M. A., & Zebiak, S. E. (1996). An Ocean dynamical thermostat. *Journal of Climate*, *9*(9), 2190–2196. https://doi.org/10.1175/1520-0442(1996)009<;2190:aodt>2.0.co;2

Cobb, K. M., Westphal, N., Sayani, H. R., Watson, J. T., Lorenzo, E. D., Cheng, H., et al. (2013). Highly variable El Niño–Southern Oscillation throughout the Holocene. *Science*, *339*(6115), 67–70. https://doi.org/10.1126/science.1228246

Collins, M., An, S.-I., Cai, W., Ganachaud, A., Guilyardi, E., Jin, F.-F., et al. (2010). The impact of global warming on the tropical Pacific Ocean and El Niño. *Nature Geoscience*, *3*(6), 391–397. https://doi.org/10.1038/ngeo868

Conroy, J. L., Overpeck, J. T., Cole, J. E., Shanahan, T. M., & Steinitz-Kannan, M. (2008). Holocene changes in eastern tropical Pacific climate inferred from a Galápagos lake sediment record. *Quaternary Science Reviews*, *27*(11–12), 1166–1180. https://doi.org/10.1016/j.quascirev.2008.02.015

Dekens, P. S., Lea, D. W., Pak, D. K., & Spero, H. J. (2002). Core top calibration of Mg/Ca in tropical foraminifera: Refining paleotemperature estimation. *Geochemistry, Geophysics, Geosystems*, *3*(4), 1–29. https://doi.org/10.1029/2001gc000200

Emile-Geay, J., Cobb, K. M., Carré, M., Braconnot, P., Leloup, J., Zhou, Y., et al. (2016). Links between tropical Pacific seasonal, interannual and orbital variability during the Holocene. *Nature Geoscience*, *9*(2), 168–173. https://doi.org/10.1038/ngeo2608

Emile-Geay, J., Cobb, K. M., Cole, J. E., Elliot, M., & Zhu, F. (2020). Past ENSO variability: Reconstructions, models, and implication. In M. J. McPhaden, A. Santoso, & W. Cai (Eds.), *El Niño Southern Oscillation in a Changing Climate* (pp. 87–118). https://doi.org/10.1002/9781119548164.ch5

Fiedler, P. C., & Talley, L. D. (2006). Hydrography of the eastern tropical Pacific: A review. *Progress in Oceanography*, *69*(2–4), 143–180. https://doi.org/10.1016/j.pocean.2006.03.008

Ford, H. L., McChesney, C. L., Hertzberg, J. E., & McManus, J. F. (2018). A deep eastern equatorial Pacific thermocline during the Last Glacial Maximum. *Geophysical Research Letters*, *45*(21), 11806–11816. https://doi.org/10.1029/2018gl079710

Ford, H. L., Ravelo, A. C., & Polissar, P. J. (2015). Reduced El Niño–Southern Oscillation during the Last Glacial Maximum. *Science*, *347*(6219), 255–258. https://doi.org/10.1126/science.1258437

Glantz, M. H. (2001). In M. H. Glantz (Ed.), *Once burned, twice shy? Lessons learned from the 1997–98 El Niño*. United Nations University. Retrieved from http://collections.unu.edu/view/UNU:2374

Glaubke, R. H. (2023). rh-glaubke/QUANTIFA: QUANTIFA v2.0.0 (2.0.0) [Software]. *Zenodo*. https://doi.org/10.5281/zenodo.7775163

Glaubke, R. H., Schmidt, M. W., Hertzberg, J. E., Ward, L. G., Marcantonio, F., Schimmenti, D., & Thirumalai, K. (2024). An inconsistent ENSO response to Northern Hemisphere stadials over the last deglaciation [Dataset]. *NOAA National Centers for Environmental Information*. https://www.ncei.noaa.gov/access/paleo-search/study/39479

Glaubke, R. H., Thirumalai, K., Schmidt, M. W., & Hertzberg, J. E. (2021). Discerning changes in high-frequency climate variability using geochemical populations of individual foraminifera. *Paleoceanography and Paleoclimatology*, *36*(2), e2020PA004065. https://doi.org/10.1029/2020pa004065

Grothe, P. R., Cobb, K. M., Liguori, G., Lorenzo, E. D., Capotondi, A., Lu, Y., et al. (2020). Enhanced El Niño–Southern Oscillation variability in recent decades. *Geophysical Research Letters*, *47*(7), e2019GL083906. https://doi.org/10.1029/2019gl083906

IPCC. (2021). *Climate change 2021: The physical science basis*. Cambridge University Press.

Karamperidou, C., Di Nezio, P. N., Timmermann, A., Jin, F.-F., & Cobb, K. M. (2015). The response of ENSO flavors to mid-Holocene climate: Implications for proxy interpretation. *Paleoceanography*, *30*(5), 527–547. https://doi.org/10.1002/2014pa002742

Koutavas, A., Demenocal, P. B., Olive, G. C., & Lynch-Stieglitz, J. (2006). Mid-Holocene El Niño–Southern Oscillation (ENSO) attenuation revealed by individual foraminifera in eastern tropical Pacific sediments. *Geology*, *34*(12), 993–996. https://doi.org/10.1130/g22810a.1

Koutavas, A., & Joanides, S. (2012). El Niño–Southern Oscillation extrema in the Holocene and Last Glacial Maximum. *Paleoceanography*, *27*(4), PA4208. https://doi.org/10.1029/2012pa002378

Leduc, G., Vidal, L., Cartapanis, O., & Bard, E. (2009). Modes of eastern equatorial Pacific thermocline variability: Implications for ENSO dynamics over the last glacial period. *Paleoceanography*, *24*(3), PA3202. https://doi.org/10.1029/2008pa001701

Lee, S., L'Heureux, M., Wittenberg, A. T., Seager, R., O'Gorman, P. A., & Johnson, N. C. (2022). On the future zonal contrasts of equatorial Pacific climate: Perspectives from observations, simulations, and theories. *Npj Climate and Atmospheric Science*, *5*(1), 82. https://doi.org/10.1038/s41612-022-00301-2

L'Heureux, M. L., Levine, A. F. Z., Newman, M., Ganter, C., Luo, J., Tippett, M. K., & Stockdale, T. N. (2020). ENSO prediction. In M. J. McPhaden, A. Santoso, & W. Cai (Eds.), *El Niño Southern Oscillation in a Changing Climate* (pp. 227–246). https://doi.org/10.1002/9781119548164.ch10

Liu, W., Pinto, D. D. C., Fedorov, A., & Zhu, J. (2023). The impacts of a weakened Atlantic meridional overturning circulation on ENSO in a warmer climate. *Geophysical Research Letters*, *50*(8), e2023GL103025. https://doi.org/10.1029/2023gl103025

Liu, Z. (2002). A simple model study of ENSO suppression by external periodic forcing. *Journal of Climate*, *15*(9), 1088–1098. https://doi.org/10.1175/1520-0442(2002)015<;1088:asmsoe>2.0.co;2

Liu, Z., Lu, Z., Wen, X., Otto-Bliesner, B. L., Timmermann, A., & Cobb, K. M. (2014). Evolution and forcing mechanisms of El Niño over the past 21,000 years. *Nature*, *515*(7528), 550–553. https://doi.org/10.1038/nature13963

Loveley, M. R., Marcantonio, F., Wisler, M. M., Hertzberg, J. E., Schmidt, M. W., & Lyle, M. (2017). Millennial-scale iron fertilization of the eastern equatorial Pacific over the past 100,000 years. *Nature Geoscience*, *10*(10), 760–764. https://doi.org/10.1038/ngeo3024

Lu, Z., Liu, Z., & Zhu, J. (2016). Abrupt intensification of ENSO forced by deglacial ice-sheet retreat in CCSM3. *Climate Dynamics*, *46*(5–6), 1877–1891. https://doi.org/10.1007/s00382-015-2681-3

Lu, Z., Liu, Z., Zhu, J., & Cobb, K. M. (2018). A review of paleo El Niño-Southern Oscillation. *Atmosphere*, *9*(4), 130. https://doi.org/10.3390/atmos9040130

Luan, Y., Braconnot, P., Yu, Y., & Zheng, W. (2015). Tropical Pacific mean state and ENSO changes: Sensitivity to freshwater flux and remnant ice sheets at 9.5 ka BP. *Climate Dynamics*, *44*(3–4), 661–678. https://doi.org/10.1007/s00382-015-2467-7

Lüthi, D., Floch, M. L., Bereiter, B., Blunier, T., Barnola, J.-M., Siegenthaler, U., et al. (2008). High-resolution carbon dioxide concentration record 650,000–800,000 years before present. *Nature*, *453*(7193), 379–382. https://doi.org/10.1038/nature06949

McGregor, H. V., & Gagan, M. K. (2004). Western Pacific coral $\delta^{18}O$ records of anomalous Holocene variability in the El Niño–Southern Oscillation. *Geophysical Research Letters*, *31*(11), L11204. https://doi.org/10.1029/2004gl019972

McManus, J. F., Francois, R., Gherardi, J.-M., Keigwin, L. D., & Brown-Leger, S. (2004). Collapse and rapid resumption of Atlantic meridional circulation linked to deglacial climate changes. *Nature*, *428*(6985), 834–837. https://doi.org/10.1038/nature02494

Merkel, U., Prange, M., & Schulz, M. (2010). ENSO variability and teleconnections during glacial climates. *Quaternary Science Reviews*, *29*(1–2), 86–100. https://doi.org/10.1016/j.quascirev.2009.11.006

Mosblech, N. A. S., Bush, M. B., Gosling, W. D., Hodell, D., Thomas, L., van Calsteren, P., et al. (2012). North Atlantic forcing of Amazonian precipitation during the last ice age. *Nature Geoscience*, *5*(11), 817–820. https://doi.org/10.1038/ngeo1588

Moy, C. M., Seltzer, G. O., Rodbell, D. T., & Anderson, D. M. (2002). Variability of El Niño/Southern Oscillation activity at millennial timescales during the Holocene epoch. *Nature*, *420*(6912), 162–165. https://doi.org/10.1038/nature01194

Partin, J. W., Cobb, K. M., Adkins, J. F., Clark, B., & Fernandez, D. P. (2007). Millennial-scale trends in west Pacific warm pool hydrology since the Last Glacial Maximum. *Nature*, *449*(7161), 452–455. https://doi.org/10.1038/nature06164

Petit, J. R., Jouzel, J., Raynaud, D., Barkov, N. I., Barnola, J.-M., Basile, I., et al. (1999). Climate and atmospheric history of the past 420,000 years from the Vostok ice core, Antarctica. *Nature*, *399*(6735), 429–436. https://doi.org/10.1038/20859

Rahmstorf, S., Box, J. E., Feulner, G., Mann, M. E., Robinson, A., Rutherford, S., & Schaffernicht, E. J. (2015). Exceptional twentieth-century slowdown in Atlantic Ocean overturning circulation. *Nature Climate Change*, *5*(5), 475–480. https://doi.org/10.1038/nclimate2554

Reimi, M. A., & Marcantonio, F. (2016). Constraints on the magnitude of the deglacial migration of the ITCZ in the Central Equatorial Pacific Ocean. *Earth and Planetary Science Letters*, *453*, 1–8. https://doi.org/10.1016/j.epsl.2016.07.058

Rein, B., Lückge, A., Reinhardt, L., Sirocko, F., Wolf, A., & Dullo, W. (2005). El Niño variability off Peru during the last 20,000 years. *Paleoceanography*, *20*(4), PA4003. https://doi.org/10.1029/2004pa001099

Rodbell, D. T., Seltzer, G. O., Anderson, D. M., Abbott, M. B., Enfield, D. B., & Newman, J. H. (1999). An ~15,000-year record of El Niño-driven alluviation in southwestern Ecuador. *Science*, *283*(5401), 516–520. https://doi.org/10.1126/science.283.5401.516

Rustic, G. T., Polissar, P. J., Ravelo, A. C., & White, S. M. (2020). Modulation of late Pleistocene ENSO strength by the tropical Pacific thermocline. *Nature Communications*, *11*(1), 5377. https://doi.org/10.1038/s41467-020-19161-6

Sadekov, A. Y., Ganeshram, R., Pichevin, L., Berdin, R., McClymont, E., Elderfield, H., & Tudhope, A. W. (2013). Palaeoclimate reconstructions reveal a strong link between El Niño-Southern Oscillation and Tropical Pacific mean state. *Nature Communications*, *4*(1), 2692. https://doi.org/10.1038/ncomms3692

Salau, O. R., Schneider, B., Park, W., Khon, V., & Latif, M. (2012). Modeling the ENSO impact of orbitally induced mean state climate changes. *Journal of Geophysical Research*, *117*(C5), C05043. https://doi.org/10.1029/2011jc007742

Schimmenti, D., Marcantonio, F., Hayes, C. T., Hertzberg, J. E., Schmidt, M. W., & Sarao, J. (2022). Insights into the deglacial variability of phytoplankton community structure in the eastern equatorial Pacific Ocean using [^{231}Pa/^{230}Th]xs and opal-carbonate fluxes. *Nature Scientific Reports*, *12*(1), 22258. https://doi.org/10.1038/s41598-022-26593-1

Schmidt, M. W., Chang, P., Hertzberg, J. E., Them, T. R., Ji, L., J, L., & Otto-Bliesner, B. L. (2012). Impact of abrupt deglacial climate change on tropical Atlantic subsurface temperatures. *Proceedings of the National Academy of Sciences*, *109*(36), 14348–14352. https://doi.org/10.1073/pnas.1207806109

Shakun, J. D., Clark, P. U., He, F., Marcott, S. A., Mix, A. C., Liu, Z., et al. (2012). Global warming preceded by increasing carbon dioxide concentrations during the last deglaciation. *Nature*, *484*(7392), 49–54. https://doi.org/10.1038/nature10915

Solan, M., Ward, E. R., White, E. L., Hibberd, E. E., Cassidy, C., Schuster, J. M., et al. (2019). Worldwide measurements of bioturbation intensity, ventilation rate, and the mixing depth of marine sediments. *Scientific Data*, *6*(1), 58. https://doi.org/10.1038/s41597-019-0069-7

Them, T. R., Schmidt, M. W., & Lynch-Stieglitz, J. (2015). Millennial-scale tropical atmospheric and Atlantic Ocean circulation change from the Last Glacial Maximum and Marine Isotope Stage 3. *Earth and Planetary Science Letters*, *427*, 47–56. https://doi.org/10.1016/j.epsl.2015.06.062

Thirumalai, K., DiNezio, P. N., Tierney, J. E., Puy, M., & Mohtadi, M. (2019). An El Niño Mode in the glacial Indian Ocean? *Paleoceanography and Paleoclimatology*, *34*(8), 1316–1327. https://doi.org/10.1029/2019pa003669

Thirumalai, K., Partin, J. W., Jackson, C. S., & Quinn, T. M. (2013). Statistical constraints on El Niño Southern Oscillation reconstructions using individual foraminifera: A sensitivity analysis. *Paleoceanography*, *28*(3), 401–412. https://doi.org/10.1002/palo.20037

Timmermann, A., Lorenz, S. J., An, S.-I., Clement, A., & Xie, S.-P. (2007). The effect of orbital forcing on the mean climate and variability of the tropical Pacific. *Journal of Climate*, *20*(16), 4147–4159. https://doi.org/10.1175/jcli4240.1

Timmermann, A., Okumura, Y., An, S.-I., Clement, A., Dong, B., Guilyardi, E., et al. (2007). The influence of a weakening of the Atlantic meridional overturning circulation on ENSO. *Journal of Climate*, *20*(19), 4899–4919. https://doi.org/10.1175/jcli4283.1

Tudhope, A. W., Chilcott, C. P., McCulloch, M. T., Cook, E. R., Chappell, J., Ellam, R. M., et al. (2001). Variability in the El Niño-Southern Oscillation through a glacial-interglacial cycle. *Science*, *291*(5508), 1511–1517. https://doi.org/10.1126/science.1057969

Wengel, C., Lee, S.-S., Stuecker, M. F., Timmermann, A., Chu, J.-E., & Schloesser, F. (2021). Future high-resolution El Niño/Southern Oscillation dynamics. *Nature Climate Change*, *11*(9), 758–765. https://doi.org/10.1038/s41558-021-01132-4

White, S. M., Ravelo, A. C., & Polissar, P. J. (2018). Dampened El Niño in the early and mid-Holocene due to insolation-forced warming/deepening of the thermocline. *Geophysical Research Letters*, *45*(1), 316–326. https://doi.org/10.1002/2017gl075433

Yang, Q., Dixon, T. H., Myers, P. G., Bonin, J., Chambers, D., van den Broeke, M. R., et al. (2016). Recent increases in Arctic freshwater flux affects Labrador Sea convection and Atlantic overturning circulation. *Nature Communications*, *7*(1), 10525. https://doi.org/10.1038/ncomms10525

Zhang, W., Dodson, J., Chang, M., & Li, G. (2021). Hydrological changes related to ENSO-like states during the last deglaciation in central eastern China. *Paleoceanography and Paleoclimatology*, *36*(10), e2021PA004279. https://doi.org/10.1029/2021pa004279

Zuo, H., Balmaseda, M. A., Tietsche, S., Mogensen, K., & Mayer, M. (2019). The ECMWF operational ensemble reanalysis–analysis system for ocean and sea ice: A description of the system and assessment. *Ocean Science*, *15*(3), 779–808. https://doi.org/10.5194/os-15-779-2019

References From the Supporting Information

Cai, W., Wang, G., Dewitte, B., Wu, L., Santoso, A., Takahashi, K., et al. (2018). Increased variability of eastern Pacific El Niño under greenhouse warming. *Nature*, *564*(7735), 201–206. https://doi.org/10.1038/s41586-018-0776-9

Cai, W., Santoso, A., Collins, M., Dewitte, B., Karamperidou, C., Kug, J.-S., et al. (2021). Changing El Niño–Southern Oscillation in a warming climate. *Nature Reviews Earth & Environment*, *2*(9), 1–17. https://doi.org/10.1038/s43017-021-00199-z

Chen, S., Hoffmann, S. S., Lund, D. C., Cobb, K. M., Emile-Geay, J., & Adkins, J. F. (2016). A high-resolution speleothem record of western equatorial Pacific rainfall: Implications for Holocene ENSO evolution. *Earth and Planetary Science Letters*, *442*, 61–71. https://doi.org/10.1016/j.epsl.2016.02.050

Freund, M. B., Henley, B. J., Karoly, D. J., McGregor, H. V., Abram, N. J., & Dommenget, D. (2019). Higher frequency of Central Pacific El Niño events in recent decades relative to past centuries. *Nature Geoscience*, *12*(6), 450–455. https://doi.org/10.1038/s41561-019-0353-3

Heede, U. K., & Fedorov, A. V. (2023). Towards understanding the robust strengthening of ENSO and more frequent extreme El Niño events in CMIP6 global warming simulations. *Climate Dynamics*, *61*(5–6), 3047–3060. https://doi.org/10.1007/s00382-023-06856-x

Spezzaferri, S., Kucera, M., Pearson, P. N., Wade, B. S., Rappo, S., Poole, C. R., et al. (2015). Fossil and genetic evidence for the polyphyletic nature of the planktonic foraminifera "*Globigerinoides*", and description of the new genus *Trilobatus*. *PLoS One*, *10*(5), e0128108. https://doi.org/10.1371/journal.pone.0128108

Thunell, R. C., & Reynolds, L. A. (1984). Sedimentation of planktonic foraminifera: Seasonal changes in species flux in the Panama Basin. *Micropaleontology*, *30*(3), 243. https://doi.org/10.2307/1485688